applied sciences

MDPI

Article

Theoretical and Numerical Study on Buongiorno's Model with a Couette Flow of a Nanofluid in a Channel with an Embedded Cavity

Eugenia Rossi di Schio [1,*], Andrea Natale Impiombato [1], Abderrahim Mokhefi [2] and Cesare Biserni [1]

[1] Department of Industrial Engineering, Alma Mater Studiorum—University of Bologna, Viale Risorgimento 2, 40136 Bologna, Italy; andrea.impiombato@gmail.com (A.N.I.); cesare.biserni@unibo.it (C.B.)
[2] Mechanics, Modeling and Experimentation Laboratory L2ME, Faculty of Technology, Bechar University, B.P. 417, Bechar 08000, Algeria; abderrahim.mokhefi@univ-bechar.dz
* Correspondence: eugenia.rossidischio@unibo.it; Tel.: +39-0512093294

Abstract: In the present paper, the fluid flow and heat transfer of a nanofluid are numerically investigated. More specifically, reference is made to a nanofluid, described by means of Buongiorno's model, subjected to Couette flow. The considered domain consists of a channel that displays a cavity shortly after the inlet section. The transport model for the nanofluid, that is the mass conservation, momentum, and nanoparticles equation, is written in a dimensionless form and solved by employing the software package Comsol Multiphysics. Many ideas emerged from this work: the visualization of the velocity stream function, the dimensionless temperature, and nanoparticle concentration fields are provided, as a function of the governing parameters: Reynolds, Peclet, Lewis, Brownian diffusivity number, and thermophoretic diffusivity number. Concerning the nanofluid typical effects, the thermophoretic diffusion seems to affect the solution much more than the Brownian diffusion. The Nusselt number on the upper wall is calculated as well, and the results show that it proves to be, in most of the considered cases, an increasing function of the Reynolds number. Moreover, concerning the Nusselt number, the Brownian diffusion effects are shown to be negligible.

Keywords: nanofluid; Bongiorno's model; Couette flow; vortex; forced convection; finite element analysis

Citation: Rossi di Schio, E.; Impiombato, A.N.; Mokhefi, A.; Biserni, C. Theoretical and Numerical Study on Buongiorno's Model with a Couette Flow of a Nanofluid in a Channel with an Embedded Cavity. *Appl. Sci.* **2022**, *12*, 7751. https://doi.org/10.3390/app12157751

Received: 27 June 2022
Accepted: 29 July 2022
Published: 1 August 2022

1. Introduction

The term "nanofluid" was first coined by Choi and Eastman [1,2] in 1995. Originally, the term described nanometer-sized copper particles dispersed in water to improve their thermal conductivity. Today, a nanofluid can be more accurately intended as an engineered colloidal suspension of nanoparticles into a base fluid. Nanofluids have shown a promising future as thermal fluids for various heat transfer applications [3]: in solar collectors [4,5], to enhance the heat-transfer coefficient of solar water heaters or to improve the capacity of thermal energy storage systems; and in the area of refrigeration, to enhance the performance of refrigeration systems. Later, many authors (see for example refs. [6–10]) studied the nanofluid flow and discussed their heat transfer performance. In the literature, a widely employed approach to describe the features of a nanofluid is the so-called Buongiorno model, which relies on the assumptions: (i) the flow is incompressible, (ii) there are no chemical reactions at nanofluids, (iii) external forces are negligible, (iv) the mixture is considered to be diluted, (v) viscous dissipation is negligible, (vi) radiation heat transfer is negligible, (vii) nanoparticles and base fluid are located in thermal equilibrium.

More specifically, Buongiorno presented the following seven mechanisms of slip between nanoparticle and fluid [11]: Inertia, Brownian diffusion, Thermophoresis, Diffusiophoresis, Magnus effect, Fluid Drainage, and Gravity settling. It is worth mentioning that the above-mentioned phenomena can produce a relative velocity between the base

fluid and nanoparticles, that is, water. He also suggested a two-component four-equation nonhomogeneous equilibrium model for three basic equations: mass, momentum, and heat transfer. Furthermore, a comparison of length scales and the nanoparticle turbulent eddy time demonstrated that, in the presence of turbulent eddies, the nanoparticle moves with the base fluid homogeneously. As a consequence, the turbulence intensity effect is also double. The presence of turbulence in the flow, which prevents the agglomeration of particles, decreases the discrepancy between experimental and numerical results. Hence, the results obtained from an analysis of Buongiorno's two-phase model are likely to be more accurate.

In this context, Azimikivi H. et al. [12] recount the effects of the rib shape with constant height, width and pitch, and nanoparticle diameter on natural convection heat transfer of low turbulence flow of AL2O3-water nanofluid inside a square cavity based on Buongiorno's model. The steady Cu-water nanofluid flow in the presence of a magnetic field has been numerically investigated by Rawat S.K. et al. [13] under the effects of mixed convection, thermal radiation, and chemical reaction. Besides this, the modeled nanofluid problem is characterized by a single-phase nanofluid model (i.e., Tiwari and Das's model) and a two-phase mixture nanofluid model (i.e., Buongiorno's model) together with the Cattaneo–Christov Double diffusion model.

In addition, according to Buongiorno's model, many papers have examined the convection of a nanofluid in a cavity or in a channel with an embedded cavity. In this regard, the forced convection heat transfer of a nanofluid in a channel has been widely investigated in refs. [14,15], while the mixed convection of a nanofluid (with various types of nanoparticles) in an open cavity has been pointed out by Mehrez et al. in ref. [16]. The single phase model has been employed to investigate the Couette forced convection of a nanofluid in ref. [17]: the governing PDEs are reduced to ODEs using a similarity transformation, and then analytically solved. The recent literature has paid attention, especially, to mixed and free convention, or, concerning forced convection, to the presence of MHD effects, as in refs. [18–20]. On the contrary, recently, the analysis of vortex formation in the case of laminar flow of a Newtonian fluid, flowing in a duct with an embedded cavity has been studied in ref. [21], where a brief analysis of the recent literature on the vortex formation in cavities is reported as well. In this context, the motivation in the current work is that flow of nanofluid over a channel/embedded cavity has been extensively discussed in the past by many authors, yet none of them made an attempt to combine the forced convection of a two-phase mixture of nanofluid with Couette flow.

More in detail, in the present paper, attention is paid to the Couette laminar flow of a nanofluid in a channel that encapsulates an embedded cavity. The nanofluid is described by employing the two-phase mixture model introduced by Buongiorno, and the presented equations are written in a dimensionless form and solved numerically by employing the commercial software package Comsol Multiphysics, based on a Galerkin finite element method. The obtained solution is shown to depend on the Reynolds number, the Peclet number, the Lewis number, the Brownian motion coefficient, and the thermophoresis coefficient. The dependence of the solution and of the Nusselt number on the parameters is then investigated and discussed.

2. Mathematical Model

Let us refer to the geometry sketched in Figure 1, that is, a channel with an embedded open cavity. The characteristic lengths of the geometry under consideration are evidenced in the figure (the geometry was built according to the size of the inlet channel H).

In accordance with Buongiorno's model [11], let us consider the nanofluid as a two-component mixture (base fluid plus nanoparticles) with the flowing assumption: (i) incompressible flow, (ii) no chemical reactions, (iii) negligible external forces, (iv) dilute the mixture, (v) negligible viscous dissipation, (vi) negligible radiative heat transfer, (vii) nanoparticles and base fluid locally in thermal equilibrium. Definitely, in accordance also

with Hussain and Ahmed [18], the transport model for the nanofluid is described by the following system of equations:

Continuity equation

$$\frac{\partial U}{\partial X} + \frac{\partial V}{\partial Y} = 0 \tag{1}$$

Momentum equations in X and Y direction

$$\rho\left(U\frac{\partial U}{\partial X} + V\frac{\partial U}{\partial Y}\right) = -\frac{\partial P}{\partial X} + \mu\left(\frac{\partial^2 U}{\partial X^2} + \frac{\partial^2 U}{\partial Y^2}\right) \tag{2}$$

$$\rho\left(U\frac{\partial V}{\partial X} + V\frac{\partial V}{\partial Y}\right) = -\frac{\partial P}{\partial Y} + \mu\left(\frac{\partial^2 V}{\partial X^2} + \frac{\partial^2 V}{\partial Y^2}\right) \tag{3}$$

Energy equation

$$U\frac{\partial T}{\partial X} + V\frac{\partial T}{\partial Y} = \alpha\left(\frac{\partial^2 T}{\partial X^2} + \frac{\partial^2 T}{\partial Y^2}\right) + \delta\left\{D_B\left(\frac{\partial \phi}{\partial X}\frac{\partial T}{\partial X} + \frac{\partial \phi}{\partial Y}\frac{\partial T}{\partial Y}\right) + \frac{D_T}{T_c}\left[\left(\frac{\partial T}{\partial X}\right)^2 + \left(\frac{\partial T}{\partial Y}\right)^2\right]\right\} \tag{4}$$

Nanoparticles equation

$$U\frac{\partial \phi}{\partial X} + V\frac{\partial \phi}{\partial Y} = D_B\left(\frac{\partial^2 \phi}{\partial X^2} + \frac{\partial^2 \phi}{\partial Y^2}\right) + \frac{D_T}{T_c}\left(\frac{\partial^2 T}{\partial X^2} + \frac{\partial^2 T}{\partial Y^2}\right) \tag{5}$$

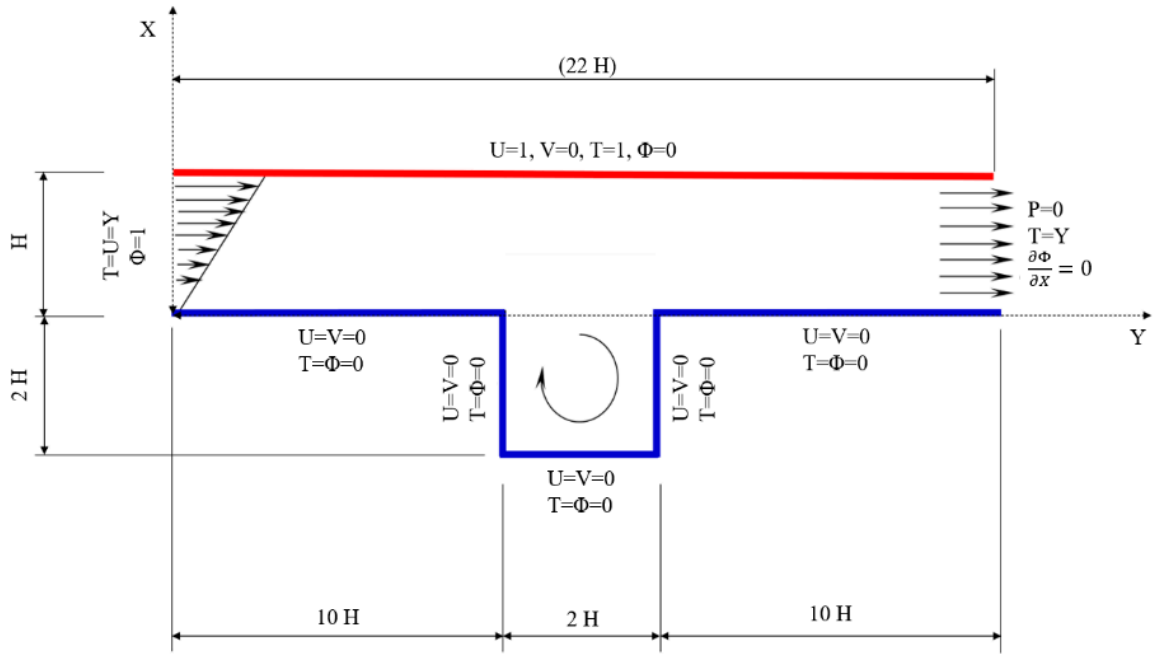

Figure 1. Domain and boundary conditions.

In Equations (1)–(5), (U, V) are the X and Y-component of the nanofluid velocity vector, P is the nanofluid pressure, T is the nanofluid temperature, ϕ is the nanoparticles concentration. These dependent variables are given as a function of the position vector (X, Y). Furthermore, ρ is the nanofluid density, μ is the dynamic viscosity, T_c is the cold temperature, $\alpha = k/(\rho\, C_p)$ is the thermal diffusivity (k is the thermal conductivity of the fluid and C_p is the fluid-specific heat constant), $\delta = (\rho\, C_p)_p/(\rho\, C_p)_f$ (p and f denotes nanoparticle

and the base fluid). Let us introduce the Brownian motion coefficient D_B, defined by the Einstein–Stokes equation, and the thermophoresis coefficient D_T, that is:

$$D_B = \frac{k_B\, T}{3\, \pi\, \mu\, d_p} \tag{6}$$

$$D_T = 0.26 \frac{k}{2k + k_p} \frac{\mu}{\rho} \phi \tag{7}$$

where k_B is Boltzmann's constant equal to $1.38064852 \times 10^{-23}$ $(\mathrm{m}^2\ \mathrm{kg})/(\mathrm{s}^2\ \mathrm{K})$, d_p is the nanoparticles diameter, k_p is the particle thermal conductivity. For the thermal energy Equation (4), non-linearities take place with both Brownian diffusion and thermophoretic diffusion.

The boundary conditions are prescribed as follows:

Inlet

$$U = U_0 \frac{Y}{H},\ V = 0,\ T = (T_h - T_c) \frac{Y}{H} + T_c, \phi = \phi_0 \tag{8}$$

Outlet

$$P = 0,\ \frac{\partial T}{\partial X} = 0 \tag{9}$$

Hot wall

$$U = U_0,\ V = 0,\ T = T_h,\ D_B \frac{\partial \phi}{\partial Y} + \frac{D_T}{T_c}\ \frac{\partial T}{\partial Y} = 0 \tag{10}$$

Horizontal cold walls

$$U = 0,\ V = 0,\ T = T_c,\ D_B \frac{\partial \phi}{\partial Y} + \frac{D_T}{T_c}\ \frac{\partial T}{\partial Y} = 0 \tag{11}$$

Vertical cold walls

$$U = 0,\ v = 0,\ T = T_c,\ D_B \frac{\partial \phi}{\partial X} + \frac{D_T}{T_c}\ \frac{\partial T}{\partial X} = 0 \tag{12}$$

In Equations (8)–(12), U_0 is the slip velocity of the hot wall and T_h is the temperature of the hot wall.

In detail, we investigate Couette flow: thus the boundary condition on the velocity field is the tangential motion of the upper surface with respect to the lower boundary. The effect of buoyancy is neglected. Moreover, the boundary conditions on the temperature foresee a uniform hot temperature T_h on the upper wall, a uniform cold temperature T_c on the lower wall and on the cavity walls, and a linearly varying temperature distribution both at the inlet and at the outlet sections. The hot and cold walls are marked with a red and blue line, respectively, in Figure 1.

On account of the dimensionless quantities

$$(x, y) = \frac{(X, Y)}{H},\ (u, v) = \frac{(U, V)}{U_0},\ p = \frac{P}{\rho\, U_0^2},\ \Theta = \frac{T - T_c}{T_h - T_c},\ \Phi = \frac{\phi}{\phi_0} \tag{13}$$

the system of Equations (1)–(5) and Equations (8)–(12) can be rewritten in the dimensionless form as follows:

$$\frac{\partial u}{\partial x} + \frac{\partial v}{\partial y} = 0 \tag{14}$$

$$u \frac{\partial u}{\partial x} + v \frac{\partial u}{\partial y} = -\frac{\partial p}{\partial x} + \frac{1}{\mathrm{Re}} \left(\frac{\partial^2 u}{\partial x^2} + \frac{\partial^2 u}{\partial y^2} \right) \tag{15}$$

$$u \frac{\partial v}{\partial x} + V \frac{\partial v}{\partial y} = -\frac{\partial p}{\partial y} + \frac{1}{\mathrm{Re}} \left(\frac{\partial^2 v}{\partial x^2} + \frac{\partial^2 v}{\partial y^2} \right) \tag{16}$$

$$u\frac{\partial \Theta}{\partial x} + v\frac{\partial \Theta}{\partial y} = \frac{1}{\mathrm{Re\,Pr}}\left\{\left(\frac{\partial^2 \Theta}{\partial x^2} + \frac{\partial^2 \Theta}{\partial y^2}\right) + N_B\left(\frac{\partial \Phi}{\partial x}\frac{\partial \Theta}{\partial x} + \frac{\partial \Phi}{\partial y}\frac{\partial \Theta}{\partial y}\right) + N_T\left[\left(\frac{\partial \Theta}{\partial x}\right)^2 + \left(\frac{\partial \Theta}{\partial y}\right)^2\right]\right\} \quad (17)$$

$$u\frac{\partial \Phi}{\partial x} + v\frac{\partial \Phi}{\partial y} = \frac{1}{\mathrm{RePrLe}}\left[\left(\frac{\partial^2 \Phi}{\partial x^2} + \frac{\partial^2 \Phi}{\partial y^2}\right) + \frac{N_T}{N_B}\left(\frac{\partial^2 \Theta}{\partial x^2} + \frac{\partial^2 \Theta}{\partial y^2}\right)\right] \quad (18)$$

$$\textit{Inlet} \qquad u = y,\ v = 0,\ \Theta = y,\ \Phi = 1 \quad (19)$$

$$\textit{Outlet} \qquad p = 0,\ \frac{\partial \Theta}{\partial x} = 0,\ \frac{\partial \Phi}{\partial x} = 0 \quad (20)$$

$$\textit{Hot wall} \qquad u = 1,\ v = 0,\ \Theta = 1,\ N_B\frac{\partial \Phi}{\partial y} + N_T\frac{\partial \Theta}{\partial y} = 0 \quad (21)$$

$$\textit{Horizontal cold wall} \qquad u = 0,\ v = 0,\ \Theta = 0,\ N_B\frac{\partial \Phi}{\partial y} + N_T\frac{\partial \Theta}{\partial y} = 0 \quad (22)$$

$$\textit{Vertical cold wall} \qquad u = 0,\ v = 0,\ \Theta = 0,\ N_B\frac{\partial \Phi}{\partial x} + N_T\frac{\partial \Theta}{\partial x} = 0 \quad (23)$$

The dimensionless boundary conditions for the velocity, temperature, and concentration fields are reported in Figure 1. In Equations (14)–(23) the following dimensionless groups have been used:

$$\textit{Reynolds number} \qquad \mathrm{Re} = \frac{\rho\, u_0\, H}{\mu} \quad (24)$$

$$\textit{Prandtl number} \qquad \mathrm{Pr} = \frac{\mu\, C_P}{k} \quad (25)$$

$$\textit{Lewis number} \qquad \mathrm{Le} = \frac{k}{\rho\, C_P\, D_B} \quad (26)$$

$$\textit{Brownian diffusivity coefficient} \qquad N_B = \frac{\delta\, D_B\, \rho\, C_P\, \phi_0}{k} \quad (27)$$

$$\textit{Thermophoretic diffusivity coefficient} \qquad N_T = \frac{\delta\, D_T\, \rho\, C_P\, \Delta T}{k\, T_c}, \quad (28)$$

where $\Delta T = T_h - T_c$.

3. Mesh and Validation

First, let us introduce, for a fixed geometry configuration (Figure 1), a sensitivity analysis of the model described through Equations (14)–(23). The constants range values used for investigating the thermophoresis and Brownian diffusion are: Pr = 6.2, $50 \leq \mathrm{Re} \leq 500$, $0.1 \leq \mathrm{Le} \leq 5$, $0.1 \leq N_B \leq 1$, and $0.1 \leq N_T \leq 1$.

The mesh used for the domain discretization is made up of quadrilateral elements. In Figure 2 some of the considered meshes are shown. In particular, in order to identify the optimal number of computational elements, the following quantities are evaluated as average in the domain of interest: velocity, temperature, particle concentration, and Nusselt number on the hot wall.

For the sake of clarity, the mean volume—related to a unit depth—quantities were evaluated according to the expression

$$\overline{\xi} = \frac{1}{\Omega}\iint \xi\, d\Omega \quad (29)$$

where ξ is the general non-dimensional quantities and Ω is the non-dimensional volume under consideration. Otherwise, the mean Nusselt number is evaluated along the hot wall by the expression

$$\overline{\mathrm{Nu}} = \frac{1}{l} \int_0^l \frac{d\Theta}{dx}\, dx \tag{30}$$

where $l = l_1 + l_2 + l_3$ is the total length of the hot wall.

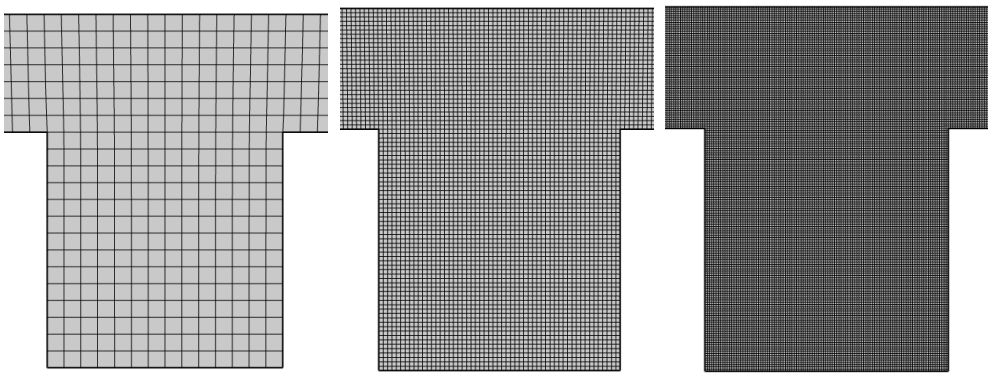

Figure 2. Mesh from coarse to fine: (**left**) 1246 elements, (**center**) 30,449 elements, (**right**) 59,520 elements.

In Table 1 the grid independence tests are reported. In the following, grid #3 will be employed.

Table 1. Grid independence test. N is the mesh elements number, $\overline{u}$ is the mean velocity, Θ is the mean temperature, Φ is the mean concentration and $\overline{\mathrm{Nu}}$ is the mean Nusselt number. The mesh validation is done for Re = 100, Pr = 6.2, NB = NT = 0.1 and Le = 10.

#	N	$\overline{u}$	$\overline{\Theta}$	$\overline{\Phi}$	$\overline{\mathrm{Nu}}$
1	1246	0.60210	0.43391	1.04165	0.98558
2	30,449	0.60199	0.43461	1.03690	0.98569
3	**59,520**	**0.60198**	**0.43463**	**1.03601**	**0.98571**
4	77,826	0.60198	0.43463	1.03600	0.98572
5	120,360	0.60198	0.43464	1.03599	0.98573

4. Results and Discussion

Let us now discuss the main features of the solutions of Equations (14)–(23). In Figures 3–6, the velocity field stream function, the isotherms, and iso-concentration lines are reported for Pr = 6.2 and by considering the variation of one parameter (Re, Le, N_B, or N_T) while the other ones, respectively, are (100, 0, 0.1, 0.1).

Figure 3 refers to different values assumed by the Reynolds number and shows that this parameter does not seem to affect sensibly the solution. Moreover, the figure shows that for increasing values of Re the stream function and isotherm gradients occur only in the channel region, not involving the open cavity, while the concentration gradients appear mainly in the cavity region.

Figure 4 refers to different values of the Lewis number and shows that for increasing values of Le the concentration vortex tends to occupy the whole cavity. Also, with reference to the channel region, for increasing values of the Lewis number, the concentration gradients tend to move close to the channel walls.

Figure 5 refers to different values of the Brownian diffusivity coefficient, showing that the solution is not strongly affected by this parameter: in fact, slight differences appear not only in the stream function distribution but also in the temperature and in the concentration distribution. Finally, Figure 6 refers to different values of the thermophoretic diffusivity coefficient N_T, showing that also this parameter does not strongly affect the obtained solution.

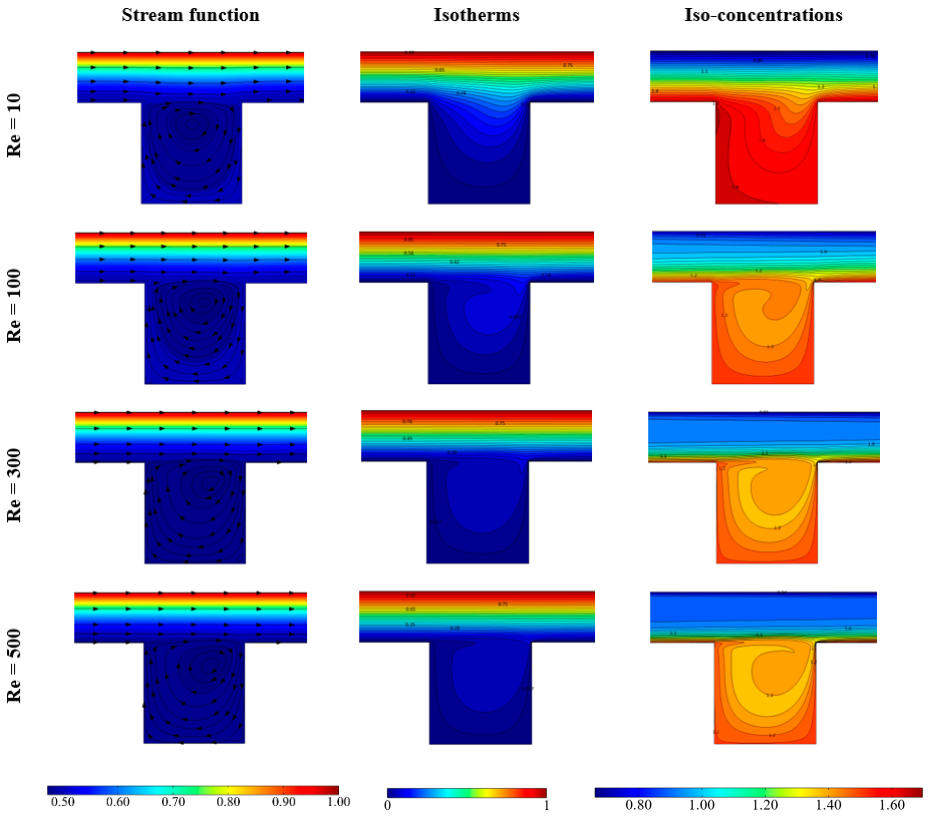

Figure 3. Stream function, Isotherms and Iso-concentration for various Reynolds number and Pr = 6.2, Le = 1, $N_B = N_T = 0.1$.

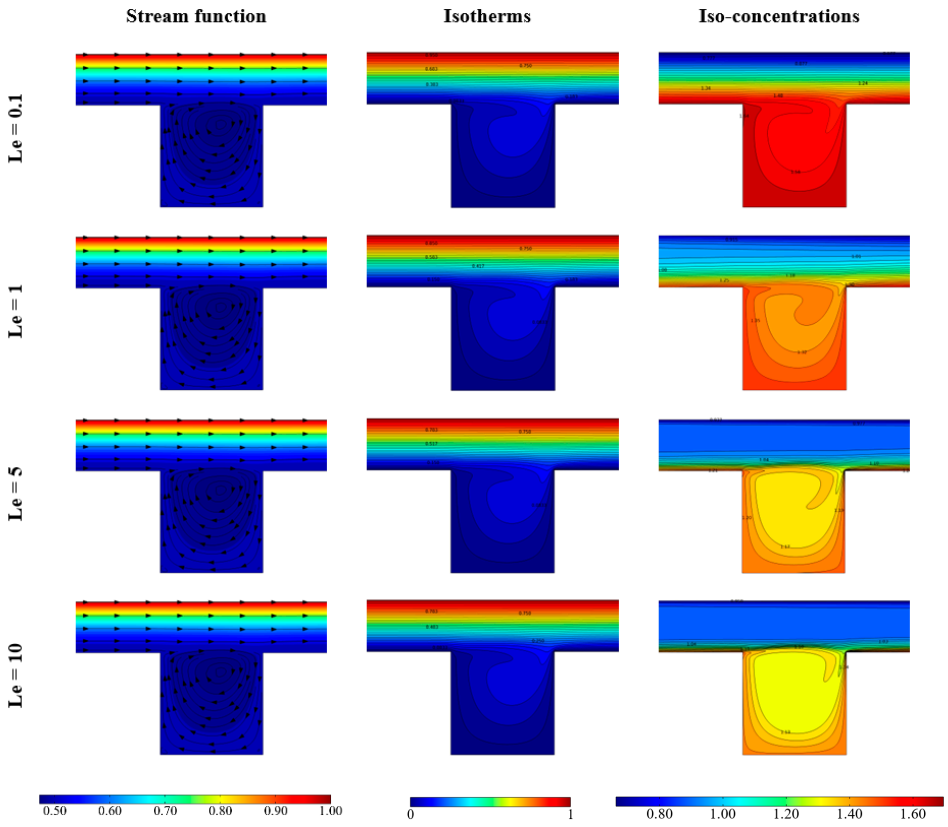

Figure 4. Stream function, Isotherms and Iso-concentration for various Lewis number and Pr = 6.2, Re = 100, $N_B = N_T = 0.1$.

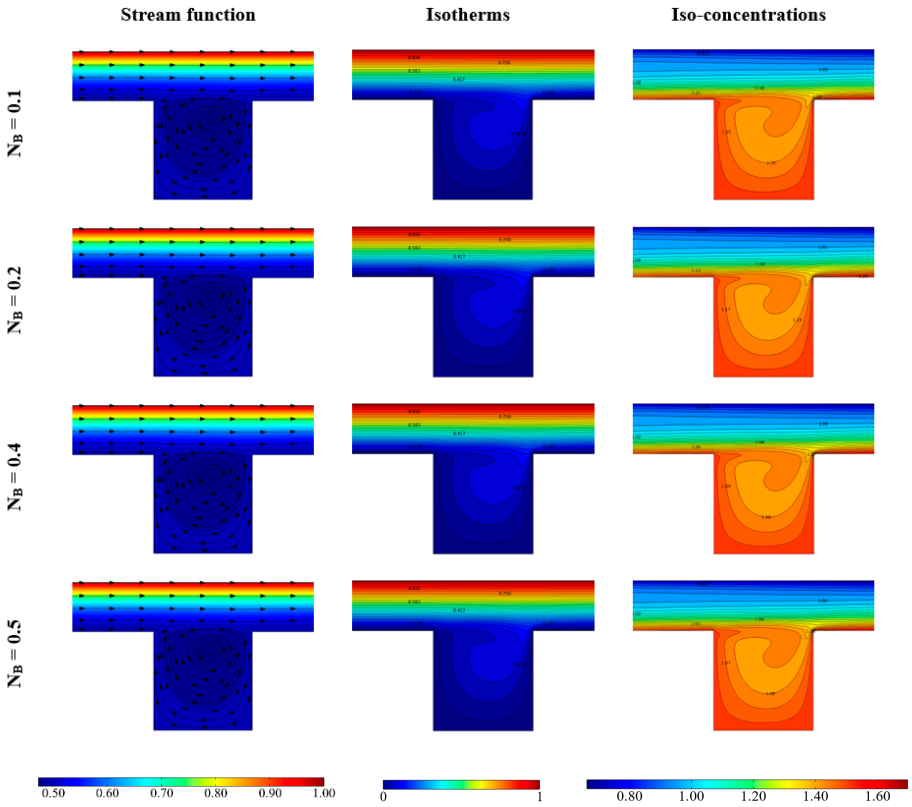

Figure 5. Stream function, Isotherms and Iso-concentration for various N_B number and Pr = 6.2, Re = 100, Le = 1, N_T = 0.1.

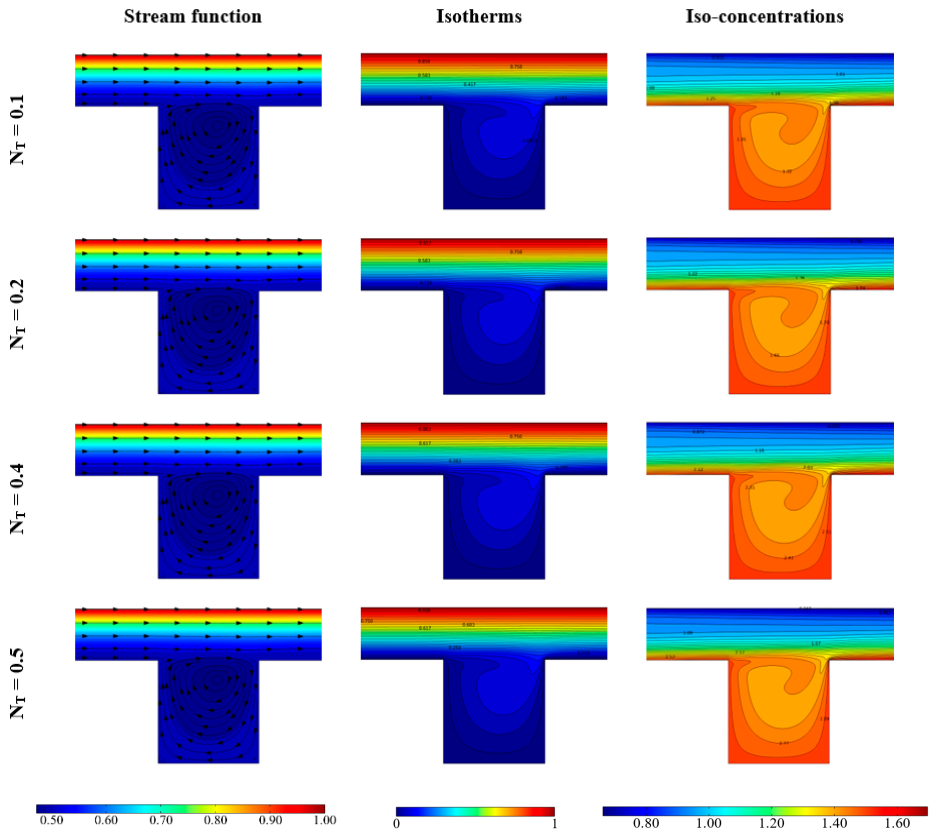

Figure 6. Stream function, Isotherms and Iso-concentration for various N_T number and Pr = 6.2, Re = 100, Le = 1, N_B = 0.1.

In Figure 7, the dimensionless concentration (lefthand frame) and the dimensionless temperature (righthand frame) are reported versus the y- coordinate at $x = (l_1 + l_2/2)/l$, and for Pr = 6.2, Le = 1, $N_B = N_T = 0.1$ and for different values assumed by the Reynolds number. The considered X-coordinate represents the vertical middle section of the cavity. The figure shows that while for Re = 10 the functions are monotonic, for higher values local minimum and maximum arise. Moreover, the concentration assumes value 1 for any considered Re at y = 0.75. This happens because the velocity value at that point is the same for all the conditions considered. Within the cavity, strong variations of the concentration occur. The dimensionless temperature distribution varies with the vertical coordinate only in the bottom cavity region, and for every mall value of the Reynolds number is a monotonic function.

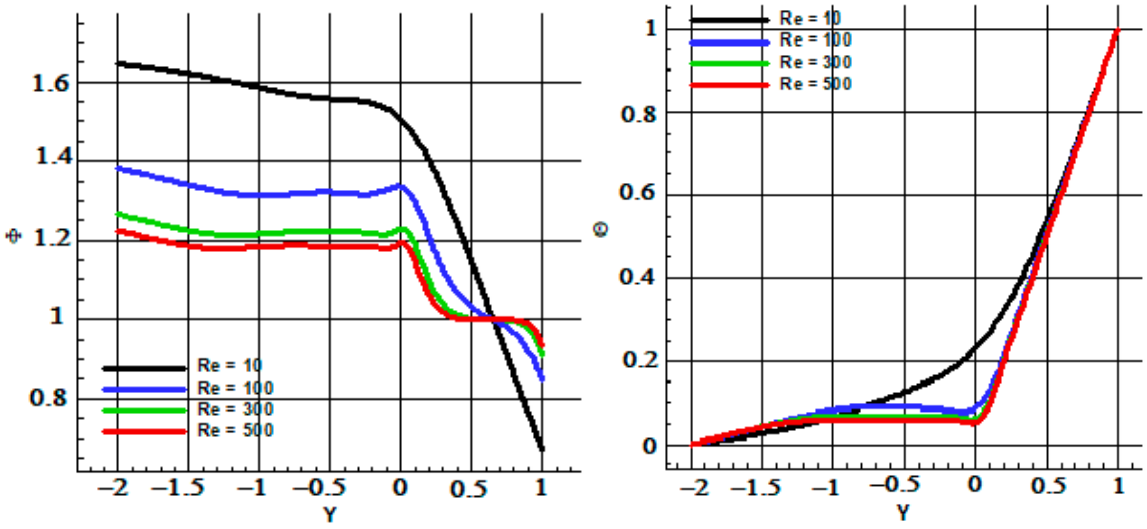

Figure 7. Concentration and temperature for different Re number and Pr = 6.2, Le = 1, $N_B = N_T = 0.1$.

In Figure 8, the y-velocity is reported versus y at the vertical middle section of the cavity, for Pr = 6.2, Le = 1, $N_B = N_T = 0.1$, and for different values assumed by the parameter Re. The figure shows that the formation of a clockwise rotating cell in the cavity occurs and that this cell occupies a bigger region of the cavity for increasing values of Re. Moreover, the maximum of the dimensionless velocity increases for increasing values of Re.

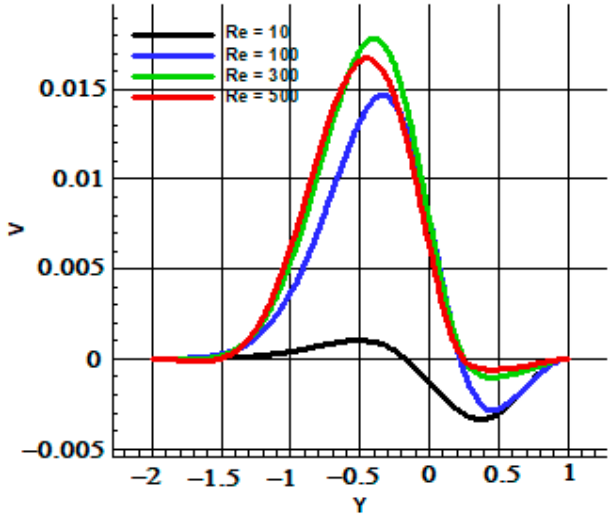

Figure 8. Y-velocity for different Re number and Pr = 6.2, Le = 1, $N_B = N_T = 0.1$.

In Figure 9 the dimensionless concentration and temperature distribution are reported as a function of the Lewis number. The righthand frame of the figure shows that the dimensionless temperature does not significantly vary: in fact, very small variations occur and are visible in the evidenced region, where the dimensionless temperature is an increasing function of Le. Moreover, a local maximum in the region close to the center of the cavity arises. On the contrary, the concentration strongly depends on the value assumed by the Lewis number. As discussed concerning Figure 7, the boundary condition imposes a concentration equal to 1 for any Le at the upper corner of the cavity.

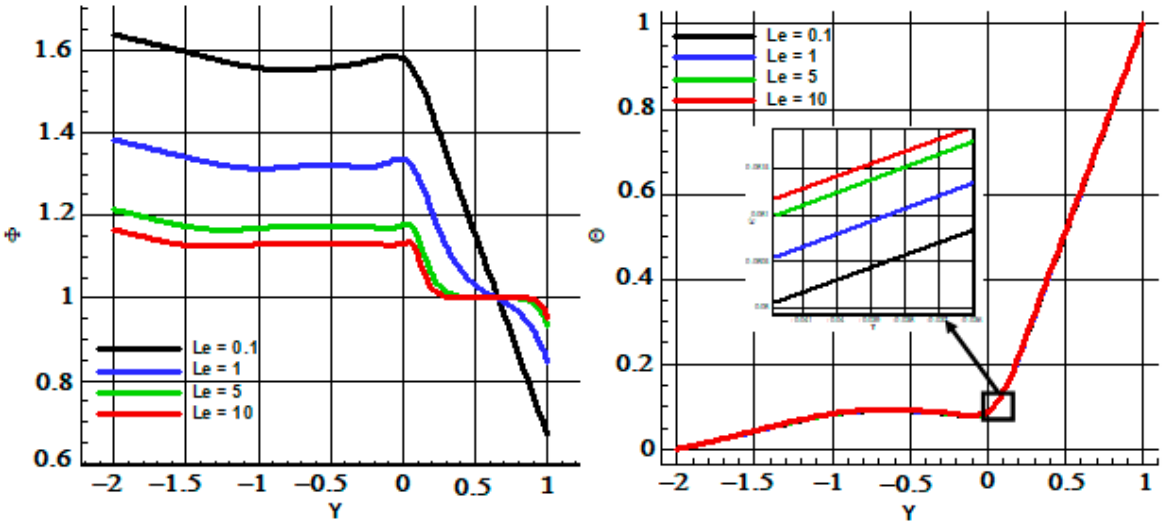

Figure 9. Concentration and temperature for different Le number and Pr = 6.2, Re = 100, N_B = N_T = 0.1.

In Figure 10, the dependence of the concentration and temperature fields on the Brownian diffusivity coefficient N_B are reported, showing that smaller values of N_B yield higher concentrations and to less uniform behavior of this function. On the contrary, N_B does not affect the trend of the dimensionless temperature.

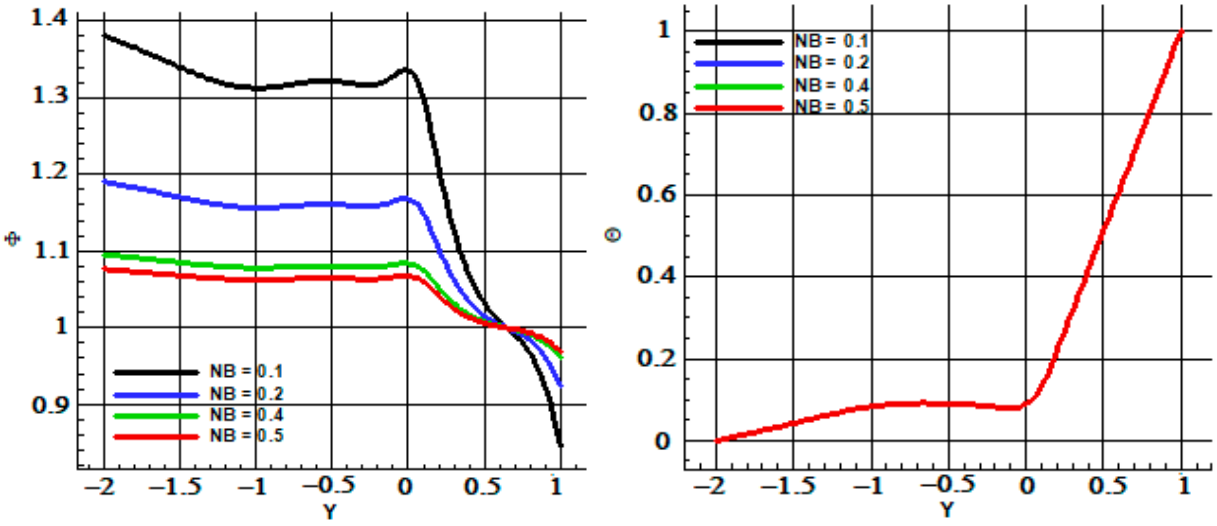

Figure 10. Concentration and temperature for different N_B number and Pr = 6.2, Re = 100, Le = 1, N_T = 0.1.

Similar considerations can be done with respect to the parameter N_T, as shown in Figure 11.

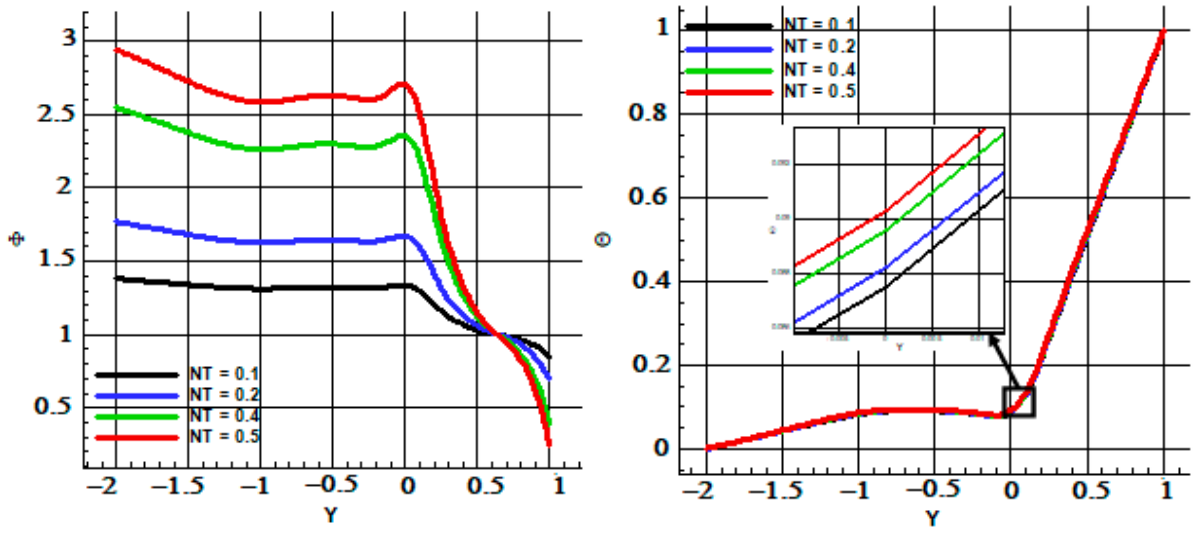

Figure 11. Concentration and temperature for different N_T number and Pr = 6.2, Re = 100, Le = 1, N_B = 0.1.

Finally, in Figures 12 and 13 the averaged Nusselt number on the hot wall is reported versus Re. Figure 12 analyzes the behavior with respect to the Brownian diffusivity coefficient (left) and to the thermophoretic diffusivity coefficient (right) and Figure 13 to the Lewis number. Figure 12 shows that the parameter N_B does not affect the behavior of the Nusselt number, while N_T and Le do, as evident in the right frame of Figure 12 and in Figure 13. In particular, the average Nusselt number is a decreasing function on N_T, while it is an increasing function of Le. It is interesting to notice that for high values of N_T, that is, N_T = 0.5, the function is not monotonic, thus displaying a minimum for Re = 100.

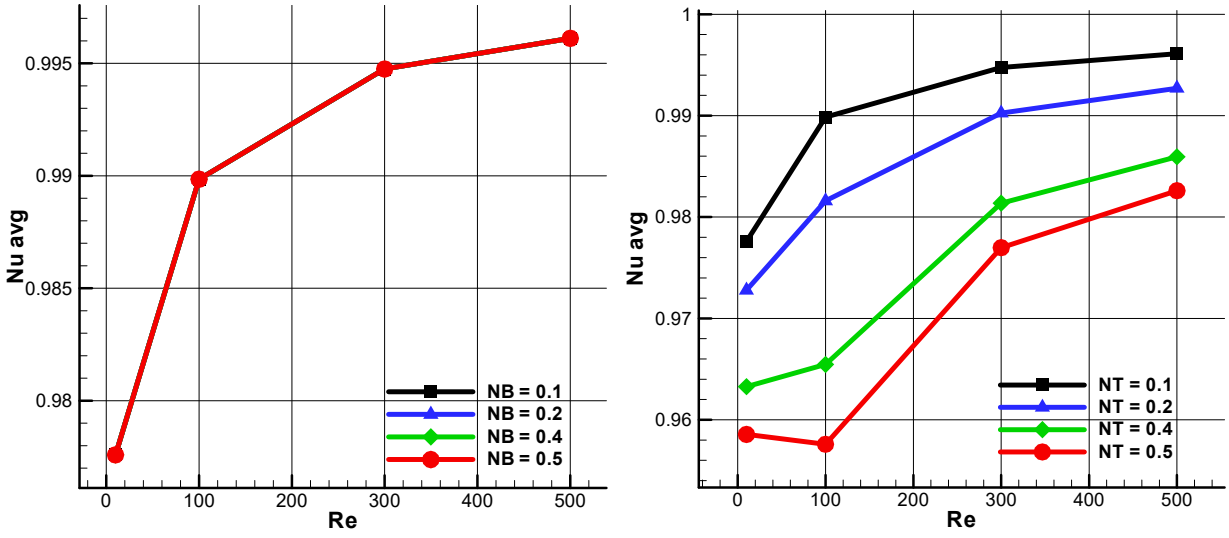

Figure 12. Average Nusselt number as a function of Re number for different N_B number and Pr = 6.2, Le = 1, N_T = 0.1 (**left**); Average Nusselt number as a function of Re number for different N_T number and Pr = 6.2, Le = 1, N_B = 0.1 (**right**).

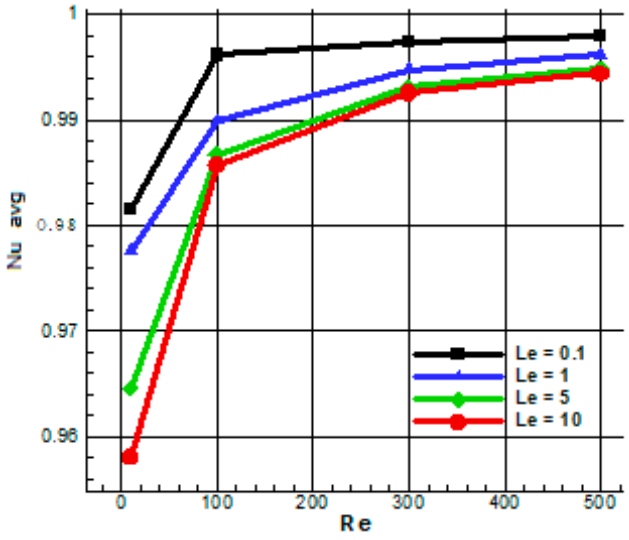

Figure 13. Average Nusselt number as a function of Re number for different Le number and Pr = 6.2, Le = 1, $N_B = N_T = 0.1$.

5. Conclusions

In the present paper, the forced convection of a nanofluid in a channel with an embedded cavity is numerically investigated. Couette flow is considered and the Buongiorno's two-phase mixture model is employed for the description of the nanofluid. The dimensionless velocity, temperature, and concentrations field are solved by employing the software package Comsol Multiphysics, as a function of the parameters Re, Pr, Le, N_B, and N_T and discussed. In particular, for increasing values of Re, the stream function and isotherm gradients occur only in the channel region, not involving the open cavity, while the concentration gradients appear mainly in the cavity region. For increasing values of the Lewis number, the concentration vortex tends to occupy the whole cavity. Moreover, with reference to the channel region, for increasing values of Le the concentration gradients tend to move close to the channel walls.

Concerning the nanofluid typical effects, the thermophoretic diffusion seems to affect the solution much more than the Brownian diffusion. Finally, the average Nusselt number on the hot wall is calculated as a function of the dimensionless parameters and discussed, showing that the Brownian diffusion effects are negligible.

Author Contributions: Conceptualization, E.R.d.S.; software, A.N.I. and A.M.; validation, all authors; formal analysis, investigation, writing—original draft preparation, writing—review and editing, all authors; supervision, E.R.d.S. and C.B. All authors have read and agreed to the published version of the manuscript.

Funding: The authors wish to thank the Italian Ministry for University.

Institutional Review Board Statement: Not applicable.

Informed Consent Statement: Not applicable.

Data Availability Statement: Not applicable.

Acknowledgments: All authors agree to the recognition of the work done.

Conflicts of Interest: The authors declare no conflict of interest.

Nomenclature

C_p	Fluid specific heat constant [J/kg K]
D_B	Brownian motion coefficient
D_T	Thermophoresis coefficient
d_P	Nanoparticles diameter
H	Cavity dimension
k	Thermal conductivity [W/m K]
k_P	Nanoparticles thermal conductivity [W/m K]
Le	Lewis number
N_B	Brownian diffusivity number
N_T	Thermophoresis number
Nu	Nusselt number
P	Nanofluid pressure [Pa]
p	Dimensionless pressure
Pr	Prandtl number
Re	Reynolds number
T	Local nanofluid temperature [K]
T_h	Hot wall temperature [K]
U	x-component velocity [m/s]
U_0	Slip velocity [m/s]
V	y-component velocity [m/s]
(u,v)	Dimensionless velocity components
X	x-coordinate [m]
Y	y-coordinate [m]
(x,y)	Dimensionless coordinates
α	Thermal diffusivity [m2/s]
Θ	Dimensionless temperature
μ	Nanofluid dynamic viscosity [Pa s]
ρ	Nanofluid density [kg/m3]
φ	Nanoparticles concentration [#/L]
Φ	Dimensionless concentration

References

1. Choi, S.U.S.; Eastman, J.A. *Enhancing Thermal Conductivity of Fluids with Nanoparticles: Technical Report ANL/MSD/CP-84938*; CONF-951135-29; Argonne National Lab.: Lemont, IL, USA, 1995.
2. Choi, S. Enhancing thermal conductivit of fluids with nanoparticles. In *Developments and Applications of Non-Newtonian Flows*; Siginer, D.A., Wang, H.P., Eds.; FED-V.231/MD-V; ASME: New York, NY, USA, 1995; Volume 66, pp. 99–105.
3. Panduro, E.A.C.; Finotti, F.; Largiller, G.; Lervåg, K.Y. A review of the use of nanofluids as heat-transfer fluids in parabolic-trough collectors. *Appl. Therm. Eng.* **2022**, *211*, 118346. [CrossRef]
4. Yan, S.R.; Aghakhani, S.; Karimipour, A. Influence of a membrane on nanofluid heat transfer and irreversibilities inside a cavity with two constant-temperature semicircular sources on the lower wall: Applicable to solar collectors. *Phys. Scr.* **2020**, *95*, 085702. [CrossRef]
5. Sheremet, M.A.; Pop, I.; Mahian, O. Natural convection in an inclined cavity with time-periodic temperature boundary conditions using nanofluids: Application in solar collectors. *Int. J. Heat Mass Transf.* **2018**, *116*, 751–761. [CrossRef]
6. Hady, F.M.; Ibrahim, F.S.; Abdel-Gaied, S.M.; Eid, M.R. Effect of heat generation/absorption on natural convective boundary-layer flow from a vertical cone embedded in a porous medium filled with a non-Newtonian nanofluid. *Int. Commun. Heat Mass Transf.* **2011**, *38*, 1414–1420. [CrossRef]
7. Alsaedi, A.; Awais, M.; Hayat, T. Effects of heat generation/absorption on stagnation point flow of nanofluid over a surface with convective boundary conditions. *Commun. Nonlinear Sci. Numer. Simul.* **2012**, *17*, 4210–4223. [CrossRef]
8. Jalilpour, B.; Jafarmadar, S.; Ganji, D.D.; Shotorban, A.B.; Taghavifar, H. Heat generation/absorption on MHD stagnation flow of nanofluid towards a porous stretching sheet with prescribed surface heat flux. *J. Mol. Liq.* **2014**, *195*, 194–204. [CrossRef]
9. Rawat, S.K.; Mishra, A.; Kumar, M. Numerical study of thermal radiation and suction effects on copper and silver water nanofluids past a vertical Riga plate. *Multidiscip. Model. Mater. Struct.* **2019**, *15*, 714–736. [CrossRef]
10. Patil, P.M.; Shashikant, A.; Hiremath, P.S. Diffusion of liquid hydrogen and oxygen in nonlinear mixed convection nanofluid flow over vertical cone. *Int. J. Hydrog. Energy* **2019**, *44*, 17061–17071. [CrossRef]
11. Buongiorno, J. Convective transport in nanofluids. *J. Heat Transf.* **2006**, *128*, 240–250. [CrossRef]

12. Azimikivi, H.; Purmahmud, N.; Mirzaee, I. Rib shape and nanoparticle diameter effects on natural convection heat transfer at low turbulence two-phase flow of AL2O3-water nanofluid inside a square cavity: Based on Buongiorno's two-phase model. *Therm. Sci. Eng. Prog.* **2020**, *20*, 100587. [CrossRef]
13. Rawat, S.K.; Upreti, H.; Kumar, M. Comparative Study of Mixed Convective MHD Cu-Water Nanofluid Flow over a Cone and Wedge using Modified Buongiorno's Model in Presence of Thermal Radiation and Chemical Reaction via Cattaneo-Christov Double Diffusion Model. *J. Appl. Comput. Mech.* **2021**, *7*, 1383–1402.
14. Ma, Y.; Mohebbi, R.; Rashid, M.M.; Yang, Z. Study of nanofluid forced convection heat transfer in a bent channel by means of lattice Boltzmann method. *Phys. Fluids* **2018**, *30*, 032001. [CrossRef]
15. Rossi di Schio, E.; Celli, M.; Barletta, A. Effects of Brownian Diffusion and Thermophoresis on the Laminar Forced Convection of a Nanofluid in a Channel. *J. Heat Transf.* **2014**, *136*, 022401. [CrossRef]
16. Mehrez, Z.; Bouterra, M.; El Cafsi, A.; Belghith, A. Heat transfer and entropy generation analysis of nanofluids flow in an open cavity. *Comput. Fluids* **2013**, *88*, 363–373. [CrossRef]
17. Makinde, O.D.; Omar, A.; Tshehla, M.S. Computational Modelling of Couette Flow of Nanofluids with Viscous Heating and Convective Cooling. *J. Comput. Math.* **2014**, *2014*, 631749. [CrossRef]
18. Ellahi, R.; Sait, S.M.; Shehzad, N.; Mobin, N. Numerical Simulation and Mathematical Modeling of Electro-Osmotic Couette–Poiseuille Flow of MHD Power-Law Nanofluid with Entropy Generation. *Symmetry* **2019**, *11*, 1038. [CrossRef]
19. Hussain, S.; Sameh, E.A.; Akbar, T. Entropy generation analysis in MHD mixed convection of hybrid nanofluid in an open cavity with a horizontal channel containing an adiabatic obstacle. *Int. J. Heat Mass Transf.* **2017**, *114*, 1054–1066. [CrossRef]
20. Seyyedi, S.M.; Dogonchi, A.S.; Hashemi-Tilehnoee, M.; Waqas, M.; Ganji, D.D. Entropy generation and economic analyses in a nanofluid filled L-shaped enclosure subjected to an oriented magnetic field. *Appl. Therm. Eng.* **2020**, *168*, 114789. [CrossRef]
21. Biserni, C.; Impiombato, A.N.; Aminhossein, J.; Rossi di Schio, E.; Semprini, G. Formation and Topology of vortices in Couette Flow over open cavities. In *E3S Web of Conferences*; EDP Sciences: Les Ulis, France, 2020; Volume 197, p. 10005.